

# Chapter 2

## Methodology

### 2.1 Calculating extinction ratio data

When observing stars through a photometric filter, only a small fraction of the bolometric stellar flux that reaches the telescope is detected. This is due to the design of the filter in question, which determines the fraction of photons detected at a given wavelength, known as the transmittance. The variation in transmittance as a function of photon wavelength is known as a transmission curve, bandpass or filter response function. Examples of filter response functions for the photometric systems are given in Figures 2.2-2.5. It is clear that range of wavelengths for which the transmittance is non-zero is very narrow when compared to the full EM spectral range.

Stars, as mentioned earlier, emit photons with wavelengths across the full EM spectrum. Figure 1.2 shows that the difference between absolute monochromatic stellar flux for different effective temperatures itself varies significantly as a function of wavelength. Therefore, when the distance to a star is unknown, a simple photometric flux measurement alone cannot easily distinguish the effect on the flux due to the intrinsic nature of the star from effects due to distance or extinction. This observational problem must therefore be mitigated before an accurate value of the extinction can be determined. The mitigation is carried out by calculating bolometric corrections.

The use of bolometric corrections requires the detailed knowledge of stellar spectra least susceptible to significant extinction, meaning, in effect, nearby stars. Knowledge of the spectrum from a reference star can allow the true spectrum of distant stars, with unknown extinction, to be calculated. The spectra of these stars can be computed by using a grid of predicted fluxes from a stellar atmosphere model, the grid being composed of the stellar parameters known to change emission in stellar atmospheres. These are effective temperature, surface gravity and metallicity. For all filter systems studied in this project, the nearby bright star Vega ( $\alpha$  Lyr) was used as the reference object. Using Vega as the reference star is the most well-known approach to photometric calibration (Casagrande & Vandenberg, 2014).

After accounting for the effect of interstellar extinction on an object's emission, its apparent magnitude in the wavelength range of a given filter  $X$ , defined as increasing from the shortest ( $\lambda_1$ ) to the longest ( $\lambda_2$ ) wavelength for which its response function is non-zero, can be calculated as:

$$m_X = -2.5 \log_{10} \left( \frac{\int_{\lambda_1}^{\lambda_2} f_\lambda (10^{-0.4A_\lambda}) S_\lambda d\lambda}{\int_{\lambda_1}^{\lambda_2} f_\lambda^0 S_\lambda d\lambda} \right) + m_X^0 \quad (2.1)$$

where  $f_\lambda$  represents the (theoretical) monochromatic flux at a given wavelength  $\lambda$  at the observer's distance from the source,  $A_\lambda$  is the extinction in  $X$  as a function of wavelength (see Equation 2.7 later for calculation of values from the Cardelli et al. (1989) law),  $S_\lambda$  represents the filter response function of  $X$ , example of which are given in Figures 2.2-2.5, and  $f_\lambda^0$  and  $m_X^0$  represent the monochromatic flux and apparent magnitude, respectively, in  $X$  of a known reference object, which is Vega in the case of the system used in this project. The use of these two well-determined observational parameters allows the remaining (uncertain) terms to be fixed to a known scale.

To derive the equation linking a bolometric correction with the extinction parameter, we start with the definition of a bolometric correction in a filter  $X$ , which is denoted by  $BC_X$ :

$$BC_X \equiv M_{\text{bol}} - M_X \quad (2.2)$$

where  $M_X$  is the absolute magnitude of the object in  $X$  and  $M_{\text{bol}}$  is its (predicted) absolute bolometric magnitude, defined relative to the Sun using:

$$M_{\text{bol}} = M_{\text{bol},\odot} - 2.5 \log_{10} \left( \frac{4\pi R^2 F_{\text{bol}}}{L_\odot} \right) \quad (2.3)$$

where  $F_{\text{bol}}$  is the bolometric stellar flux at its surface,  $R$  is the stellar radius,  $M_{\text{bol},\odot}$  is the solar absolute bolometric magnitude, which is assumed in this work to have a value of 4.75 and  $L_\odot$  is the solar luminosity, for which a value of  $3.844 \times 10^{33} \text{ erg s}^{-1}$  is used. Bolometric corrections can be expressed as a function of extinction using the definition of  $M_X$  in terms of  $m_X$  and the distance  $d$  to the source:

$$M_X = m_X - 2.5 \log_{10} \left( \left( \frac{d}{10\text{pc}} \right)^2 \right), \quad (2.4)$$

together with the equation linking flux definitions to distance:

$$f_\lambda d^2 = F_\lambda R^2 \quad (2.5)$$

where  $F_\lambda$  is the monochromatic flux at  $\lambda$  at the stellar surface. This gives the final function for a bolometric correction ( $BC$ ) for filter  $X$ :

$$\begin{aligned}
BC_X = M_{\text{bol},\odot} - m_X^0 - 2.5 \log_{10} \left( \frac{4\pi R^2 F_{\text{bol}}}{L_{\odot}} \right) \\
+ 2.5 \log_{10} \left( \frac{\int_{\lambda_1}^{\lambda_2} F_{\lambda} (10^{-0.4A_{\lambda}}) S_{\lambda} d\lambda}{\int_{\lambda_1}^{\lambda_2} f_{\lambda}^0 S_{\lambda} d\lambda} \right)
\end{aligned} \tag{2.6}$$

It should be noted that  $F_{\lambda}$  is the monochromatic spectral flux produced by the theoretical stellar atmosphere model, and varies with changes in the effective temperature, surface gravity and metallicity of the model. For a filter  $X$ , the extinction parameter  $A_X$ , equal to  $A_{\lambda}$  for the response function of filter  $X$ , is usually parametrised relative to the extinction in the well-studied Johnson- $V$  filter,  $A_V$ . To extract  $A_X$ , we use the simple relation

$$A_{\lambda} = \left( \frac{A_{\lambda}}{A_V} \right) A_V \tag{2.7}$$

together with the Cardelli et al. (1989) extinction law for  $A_{\lambda}/A_V$ , which is monochromatic and therefore must be placed within the integrand of Equation 2.6. Given that the Cardelli et al. (1989) extinction law is normalised to  $A_V$ , the value of  $A_V$  must be specified prior to the calculation of the bolometric correction. Equation 2.6 was implemented twice, once for each of two distinct  $A_V$  values (for this project these were  $A_V = 0, 1$ ). It should be noted that  $BC_X(A_V = 0)$  essentially assumes no extinction in any filter. Two output values were calculated for Equation 2.6, one for each  $A_V$  value. The difference between the two outputs was then taken to extract the extinction ratio  $A_X/A_V$ , via the following equation (Girardi et al., 2008):

$$BC_X(0) - BC_X(A_V) = (A_X/A_V) A_V \tag{2.8}$$

As demonstrated in Equation 2.8, any dependence of the  $A_X/A_V$  data on the Vega measurements or (as yet unknown or uncertain) bolometric quantities from Equation 2.6 is eliminated during the subtraction. However, effects due to the nature of the atmosphere of the stellar source on the extinction ratio will remain present, in the form of the integration of  $F_{\lambda} (10^{-0.4A_{\lambda}})$  and  $F_{\lambda}$  in the respective bolometric correction terms.

The Forbes effect (see Section 1.2.2) has an impact on the non-zero  $A_V$  value chosen for Equation 2.8 because if  $R_V$  is held constant at the standard diffuse ISM value of 3.1 (Cardelli et al., 1989), a larger  $A_V$  value implies a longer path through the ISM, and thus a stronger Forbes effect. According to Girardi et al. (2008), any significant impact from the Forbes effect on the values of  $A_X/A_V$  occurs for a chosen  $A_V \gtrsim 4$ . They found that the effect was particularly strong for stars with  $T_{\text{eff}} \lesssim 3000\text{K}$  and that, unsurprisingly, it became greater as the wavelength range covered by the filter response function increased.

Once the  $A_X/A_V$  data was calculated, functions of the three stellar parameters described in Section 1.2.1 were created and fitted to the data, with the function coefficients acting as the free parameters to be fitted. The best-fit values of these coefficients were calculated using a least-squares fit algorithm.

## 2.2 Software used

### 2.2.1 Isochrones

The isochrones used in this project were generated using the latest Bag of Stellar Tracks and Isochrones (BaSTI) web interface (Pietrinferni et al. (2004), Hidalgo et al. (2018)). The filter systems whose throughput data were employed by BaSTI to generate the fluxes for the isochrones were ACS, WFC3 and Gaia-DR2. It should be noted that the WFC3 isochrone output for BaSTI does not include flux magnitudes for the F300X filter.

To obtain isochrones from the online database, the desired range of isochrone ages, initial metallicity and photometric filter system must be specified. Therefore, the values of these quantities are shared by all stellar objects in any given isochrone. The output from the BaSTI database for each model stellar object gives the model's initial mass and current mass (i.e. after a time equal to the isochrone age), together with the logarithms of the stellar luminosity in solar units ( $\log(L/L_\odot)$ ) and of the effective temperature in K ( $\log(T_{\text{eff}})$ ), followed by the absolute magnitudes (with zero extinction) of the object in each filter of the system.

### 2.2.2 Stellar atmosphere models

To generate the predicted stellar flux, pre-calculated ATLAS9 model stellar atmosphere spectra (Kurucz, 1993). The spectra came in the form of tables incorporated wavelengths, ranging from 9 nm to 160,000 nm, with a resolution of 2 nm or less in the UV, and the predicted monochromatic flux at those wavelengths. Each table, representing one stellar spectrum, is identified by the surface gravity, effective temperature and metallicity of the stellar atmosphere producing that spectrum. Table 1 of Castelli & Kurucz (2004) contains precise details of the coverage of the model atmospheres in  $(T_{\text{eff}}, \log(g))$  parameter space, while a brief summary of the limits of the space is listed in Table 2.1. Four input metallicities were used for ATLAS9, at values of  $[\text{Fe}/\text{H}] = -2, -1, 0$  and  $0.5$ , covering the metallicities of most observed globular and open clusters. The data for each metallicity values was subject to the same  $T_{\text{eff}}$  and  $\log(g)$  coverage in ATLAS9.

Parameter / unit	Minimum	Maximum	Number of values
$T_{\text{eff}} / \text{K}$	3500	50000	76
$\log(g / \text{cm s}^{-2})$	0.0	5.0	11
[Fe/H]	-2.0	0.5	4

Table 2.1: Ranges for the input parameters for ATLAS9 atmospheric models

To make the results of this project apply to the greatest possible range of stellar types, the model atmospheres being employed must ideally be able to reproduce all observed stellar types. Since ATLAS9 atmospheres are constructed from a grid of  $T_{\text{eff}}$  and  $\log(g)$  values (Castelli & Kurucz, 2004), the simplest method of ascertaining their applicability is to obtain the  $T_{\text{eff}}$  and  $\log(g)$  values of the stellar objects which make up the isochrone.

However, the BaSTI data format for a given isochrone does not include explicit values of the surface gravities or radii of the constituent stars. Therefore, to derive the surface gravity  $g$  of a given star, we must combine Equation 1.11, to derive the stellar radius, and Equation 1.13, resulting in the following definition of  $g$ :

$$g = \frac{4\pi G M_* \sigma_{\text{SB}} T_{\text{eff}}^4}{L_*} \quad (2.9)$$

After this had been completed for all stars in an isochrone, each star had a co-ordinate in  $(T_{\text{eff}}, \log(g))$  parameter space, plus the metallicity of the overall isochrone model. These co-ordinates were then plotted over the grid of co-ordinates for which ATLAS9 spectra were available, as listed in Table 1 of Castelli & Kurucz (2004). The results are shown in Figure 2.1, using stars in isochrones with ages of 50 Myr (red points) and 12 Gyr (black points). The blue points represent the ATLAS9 model grid, which, in fact, extends to the left beyond the  $T_{\text{eff}}$ -scale presented in the figure, up to a  $T_{\text{eff}}$  value of 50,000 K.

With the exception of the very coolest, and therefore faintest, main sequence stars in the bottom right of the figure, it is clear from Figure 2.1 that the ATLAS9  $T_{\text{eff}}$ - $\log(g)$  grid covers the required parameter space for isochrones of all ages including extremely young and extremely old clusters. Any changes in the position of the isochrones in the  $(T_{\text{eff}}, \log(g))$  plane at the plotted ages due to a change in metallicity were found to have an insignificant impact on the overlap between the ATLAS9 grid and both isochrones in the  $(T_{\text{eff}}, \log(g))$  plane.

This near-complete coverage of stellar objects in isochrones at all ages allows the ATLAS9 data to be applied to the MSTO locations at all isochrone ages, which ensures the applicability of the best-fit isochrone parameter comparisons (see Section 2.4 later) to populations of all ages. Therefore, ATLAS9 is a suitable basis from which start

calculating bolometric corrections and therefore, via Equation 2.8, extinction.

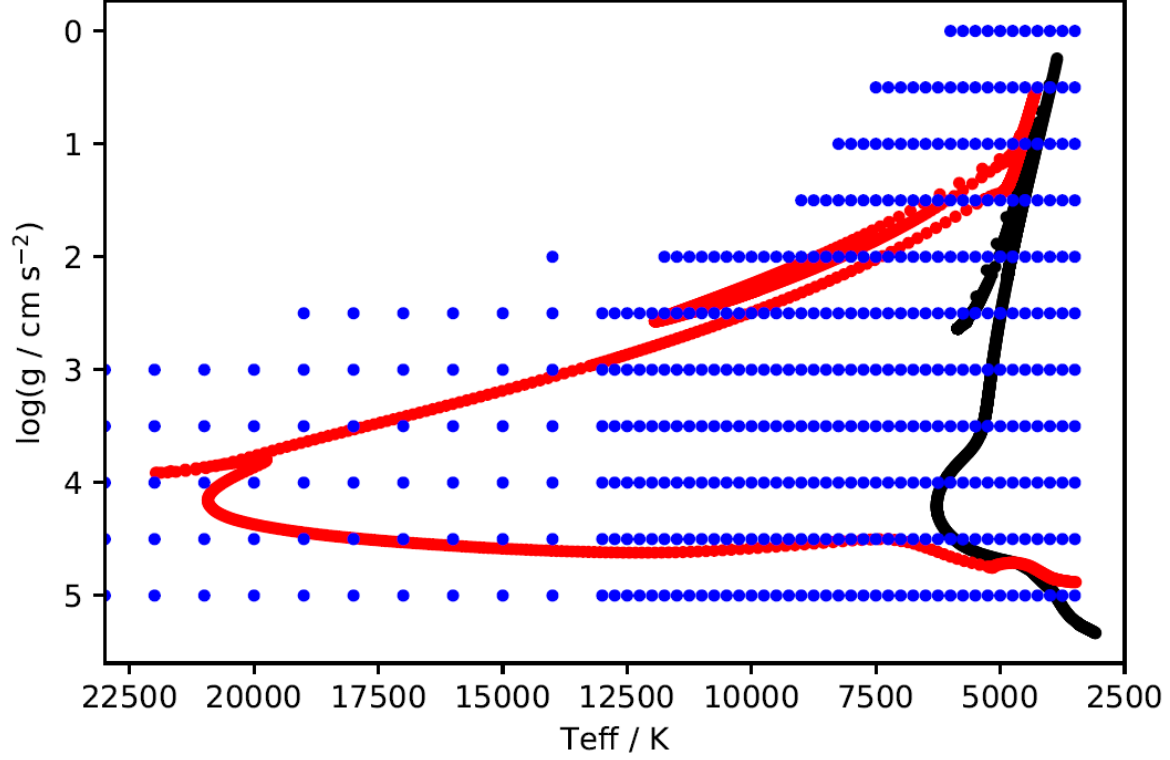


Figure 2.1:  $T_{\text{eff}}\text{-}\log(g)$  scatter plot for a BaSTI 50 Myr,  $[\text{Fe}/\text{H}] = -1$  isochrone (red), a BaSTI 12 Gyr,  $[\text{Fe}/\text{H}] = -1$  isochrone (black) and ATLAS9 model grid (blue) for  $T_{\text{eff}} \leq 23000$  K.

### 2.2.3 Programming languages

The tables of bolometric corrections were generated using a FORTRAN 77 code which incorporated Equations 2.2-2.8 and input data files with tables describing the response functions of all relevant filter systems (described in detail in Section 2.3) at the same wavelengths as those listed in the ATLAS9 model atmosphere tables, with the number of tables for each stellar metallicity value equal to the total number of  $(T_{\text{eff}}, \log(g))$  combinations available.

Once the bolometric correction tables were produced, all subsequent processes, including the subtraction required to obtain  $A_X/A_V$  shown in Equation 2.8, were written in Python 2.7 in the form of an IPython notebook. The repository containing all data, plots and programme codes for this project can be found at [https://github.com/AlexlwAstro/phd\\_work](https://github.com/AlexlwAstro/phd_work).

## 2.3 Filters studied

In this project, three broad-band filter systems were employed. Two are systems on board the Hubble Space Telescope (HST). These are the Advanced Camera for Surveys (ACS), installed in 2002 on the HST (Sarajedini et al., 2007), and the Ultraviolet Imaging Spectrograph channel of the Wide-Field Camera 3 (WFC3/UVIS), installed on the HST in 2009 (Kalirai et al., 2010; MacKenty et al., 2010). The third is the single set of three broadband filters mounted on the Gaia space observatory (Jordi et al., 2010), launched in 2013.

Examples of response functions for the three filter systems employed in this project are shown in Figures 2.2-2.5. By comparing these with the filters' information in Table 2.2, it can be seen that the exact shape of the response function has a significant impact on the observed flux, as shown in its contribution to the value of the apparent magnitude in Equation 2.1.

Reference will also be made to the Johnson-Morgan filter system (often simply known as the Johnson system) UBV Johnson & Morgan (1953), later extended as the Johnson-Cousins UBVRI Bessell (1990) system, which has been in use for decades and continues to be the standard reference for more modern filter systems. Of particular importance are the Johnson blue ( $B$ ) and yellow ( $V$ ) filters, as these formed the original benchmark for observing stellar populations and evolutionary stages.

The standard treatment of extinction is to apply a single constant value of the extinction ratio for a given filter  $X$ . This quantity is usually expressed as a fixed extinction ratio  $A_X/A_V$  of the (constant) coefficient value in the Johnson- $V$  filter, the standard visual comparison filter. This value is maintained for all stars, regardless of the different effective temperatures, metallicities or surface gravities of the different types of stars present in any given population. The wavelengths of optical light lie between 3800 Å and 7400 Å, with the  $V$  filter having a central wavelength of 5500 Å.

In Table 2.2, all the filters used for this project are listed. The name of each filter is displayed alongside its central wavelength ( $\lambda_{\text{cen}}$ ), full-width at half-maximum (FWHM) and the minimum ( $\lambda_{\text{min}}$ ) and maximum ( $\lambda_{\text{max}}$ ) detection wavelengths. Hence, when combined, these filters cover wavelengths from the soft-ultraviolet (soft-UV) to the near-infrared (NIR), including all visible wavelengths. The FWHM is defined as the difference between the lowest and highest wavelength values at which the transmittance value is half of its maximum value for the filter, typically assuming the response function can be approximated as a Gaussian distribution centred on the central wavelength. The FWHM acts as an approximate measure of the wavelength range within which the filter can be used for observations.

System	Filter	$\lambda_{\text{cen}} / \text{\AA}$	FWHM / $\text{\AA}$	$\lambda_{\text{min}} / \text{\AA}$	$\lambda_{\text{max}} / \text{\AA}$
ACS	F435W	4359	881	3610	4860
	F475W	4781	1403	3863	5563
	F555W	5413	1236	4584	6209
	F606W	5961	2255	4634	7180
	F625W	6323	1390	5446	7100
	F775W	7763	1517	6804	8632
	F814W	8117	2096	6885	9648
WFC3	F218W	2216	329	1990	2603
	F225W	2341	464	1990	2968
	F275W	2696	417	2282	3119
	F300X	2722	660	2137	4098
	F336W	3368	550	3014	3707
	F390W	3929	951	3255	4470
	F438W	4322	674	3895	4710
	F475W	4768	1482	3942	5582
	F555W	5262	1578	4381	7045
	F606W	5941	2298	4700	7204
	F625W	6274	1573	5414	7138
	F775W	7725	1454	6869	8571
	F814W	7814	1505	6978	9684
Gaia	$G$	6631	4397	3321	10515
	$G_{\text{bp}}$	5330	2530	3283	6714
	$G_{\text{rp}}$	7896	2956	6296	10637

Table 2.2: Basic properties of the filters employed in this project. See text for details. Source: <http://svo2.cab.inta-csic.es/svo/theory/fps3/index.php>



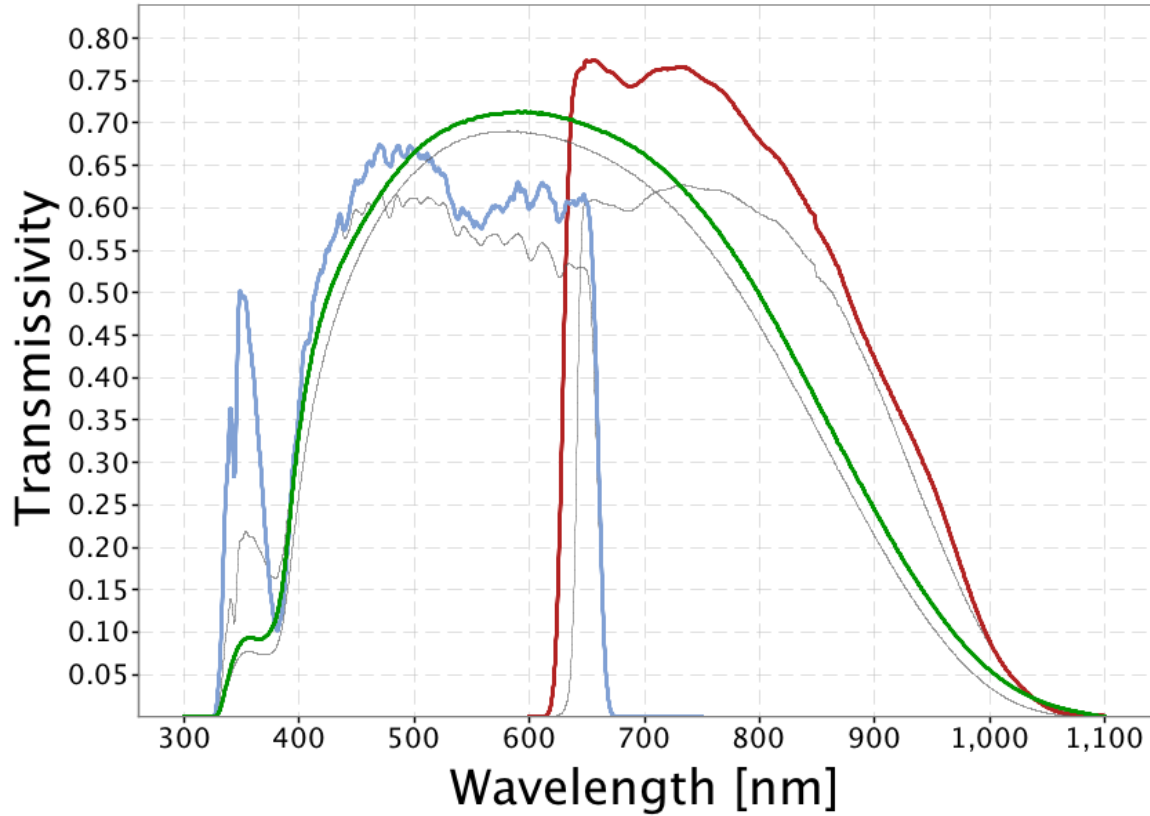


Figure 2.2: Filter response functions for Gaia photometric filters. Source: [https://www.cosmos.esa.int/web/gaia/iow\\_20180316](https://www.cosmos.esa.int/web/gaia/iow_20180316)

## 2.4 Isochrone data fitting

To match the quantities of observational datasets (with unknown extinction) and isochrones, it is necessary to correct the observational data for distance and add extinction to the isochrones. This is that standard procedure used when analysing observational data. Thus, the  $M_{\text{ext},X}$  values for the isochrones and the observational data are being compared. The functions described in Section 3.3 were then applied to the dataset of stellar objects, producing values of  $M_{\text{ext},X}$  for each filter for all objects, as is the standard for analysing observational data with unknown extinction values.

When comparing the two approaches to extinction, in order to test for any differences in projected isochrone age via the MSTO, a range of ages must be considered. A “primary” age was utilised as the true cluster isochrone age. This primary isochrone was subjected to both the function-based (FBER) and fixed extinction-ratio approaches. Two isochrones with ages equidistant from the primary were subjected to the standard fixed-extinction approach only. All four of the resulting  $M_{\text{ext},X}$  isochrones were plotted together in the four chosen CMD axes, together with the original (zero-extinction) isochrone for visual reference.

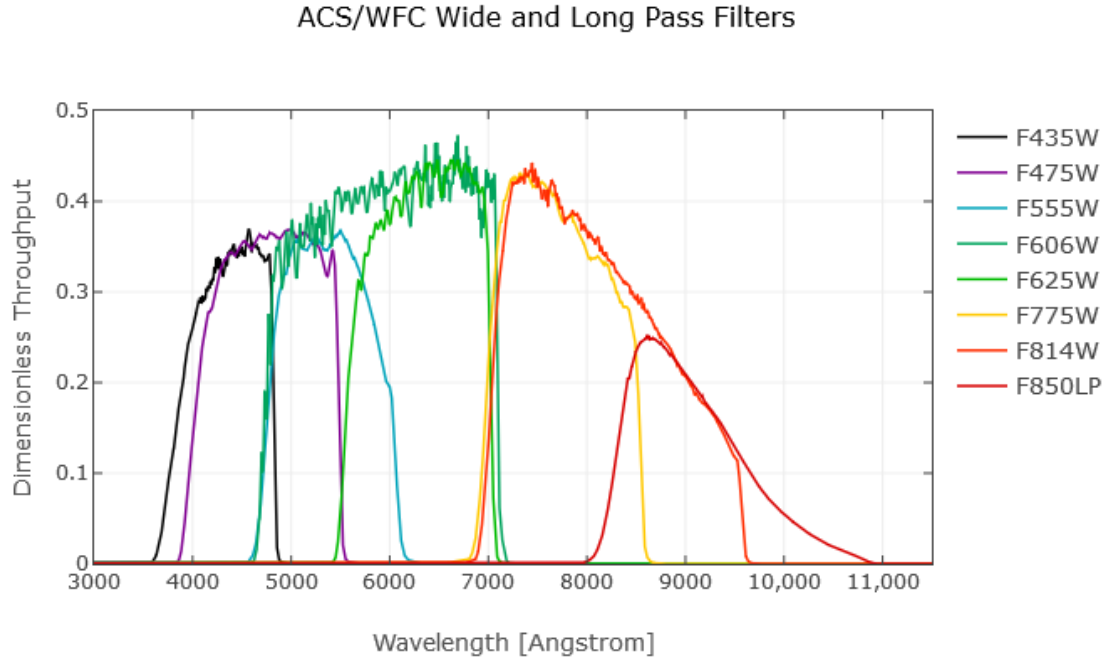


Figure 2.3: Filter response functions for wide-field ACS filters. Source: <http://www.stsci.edu/hst/acs/analysis/throughputs>

This procedure was employed for two values of  $A_X/A_V$  for the fixed-extinction treatment. Both were extracted from the ATLAS9 data tables for a  $\log(g)$  value of 5.0 to represent a main-sequence star, which is suitable when MSTO positions are being compared. Given the large number of filters studied in this project, four commonly-used CMD axes were selected to test for any effects of a  $A_X/A_V$  function. Two of these are specific to the WFC3 system, with one CMD each for ACS and Gaia.

## 2.5 Observational test case: NGC 6793

To test the effects of the two different treatments of  $A_X/A_V$  on observational data, both were employed to predict the isochrone parameters (age, [Fe/H] and  $A_V$ ) for the open cluster NGC 6793.

NGC 6793 has little information available in the literature when compared to open clusters. Three observational studies have been published which give estimates for the properties of the cluster. The basic properties for all three studies are listed in Table ???. However, it has the significant advantage of having both a very high  $A_V$  extinc-

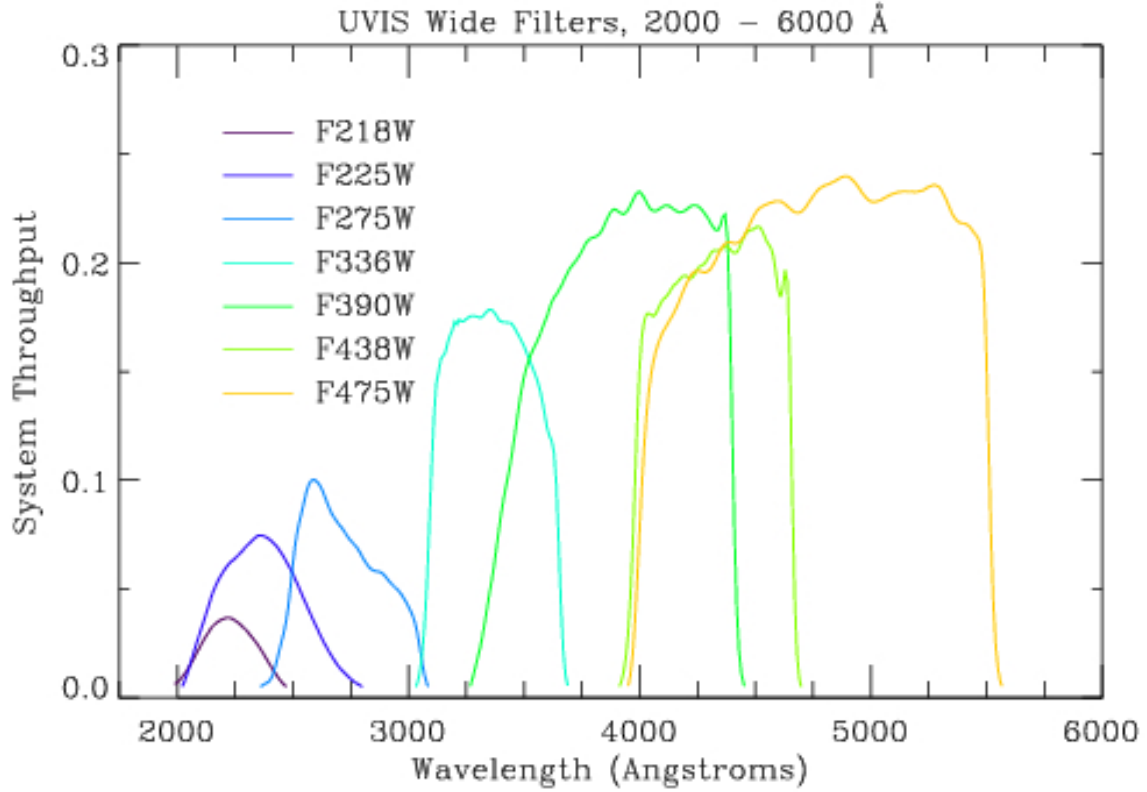


Figure 2.4: Filter response functions for wide-field WFC3 filters. Source: [http://www.stsci.edu/hst/wfc3/ins\\_performance/throughputs/UVIS\\_filterthru.html](http://www.stsci.edu/hst/wfc3/ins_performance/throughputs/UVIS_filterthru.html)

tion value among star clusters and a full set of Gaia parallax measurements for its member stars. The accurate distances to all its members allows for a higher degree of confidence in the position of the observed cluster CMD. Meanwhile, a high  $A_V$  value increases any disagreement between the extinction treatments being compared for the cluster. Consequently, any resulting disagreement in estimates of the best-fit isochrone parameters for the cluster become greater and more significant.

The Gaia DR2 dataset for NGC 6793, containing the parallaxes and apparent magnitudes (in all three Gaia filters) for 338 objects identified as belonging to the cluster, was obtained. The number of objects is greater than the 271 photometric Gaia objects found by Gaia Collaboration et al. (2018), hereafter referred to as GC18. Restrictions on the parallax measurements were implemented, by imposing a distance-based selection range centred at 600 pc, which was treated as the centre of the cluster, in line with the GC18 estimate in Table ?? . The range was decreased until the remaining sample size was approximately equal to 271. When this was implemented, the final sample of observational data for NGC 6793 contained 274 objects. Some of these objects still

Isochrone (Age/Myr , [Fe/H])	$T_{\text{eff}}$ minimum	$T_{\text{eff}}$ maximum	$\log(g)$ minimum	$\log(g)$ maximum
500,0.002	2870	9640	0.886	5.137
1000,0.002	2824	8035	1.608	5.184
5000,-1.049	3118	7112	0.456	5.318
10000,-1.049	3086	6412	0.286	5.332

Table 2.3: Ranges of effective temperature and surface gravities in selected BaSTI isochrones

Cluster property	K05	K13	GC18
Distance modulus / mag	10.73	9.399	8.894
-> distance / pc	1400	724	601
log(age / yr)	8.64	8.695	8.78
-> Age / Myr	437	495	603
$E(B - V)$ / mag	0.17	0.312	0.272
-> $A_V$ / mag (if $R_V = 3.1$ )	0.53	0.967	0.843
[Fe/H]	?	?	?
Members	? (> 3 ACSS-2.5)	133*	465 (271 with Gaia photometry)

\*number of  $1\sigma$  objects inside MWSC "cluster corona border"

Table 2.4: Observational parameters for NGC 6793, according to Kharchenko et al. (2005) (K05, WEBDA archive page), Kharchenko et al. (2013) (K13, VizieR archive page) and Gaia Collaboration et al. (2018) (GC18), respectively.

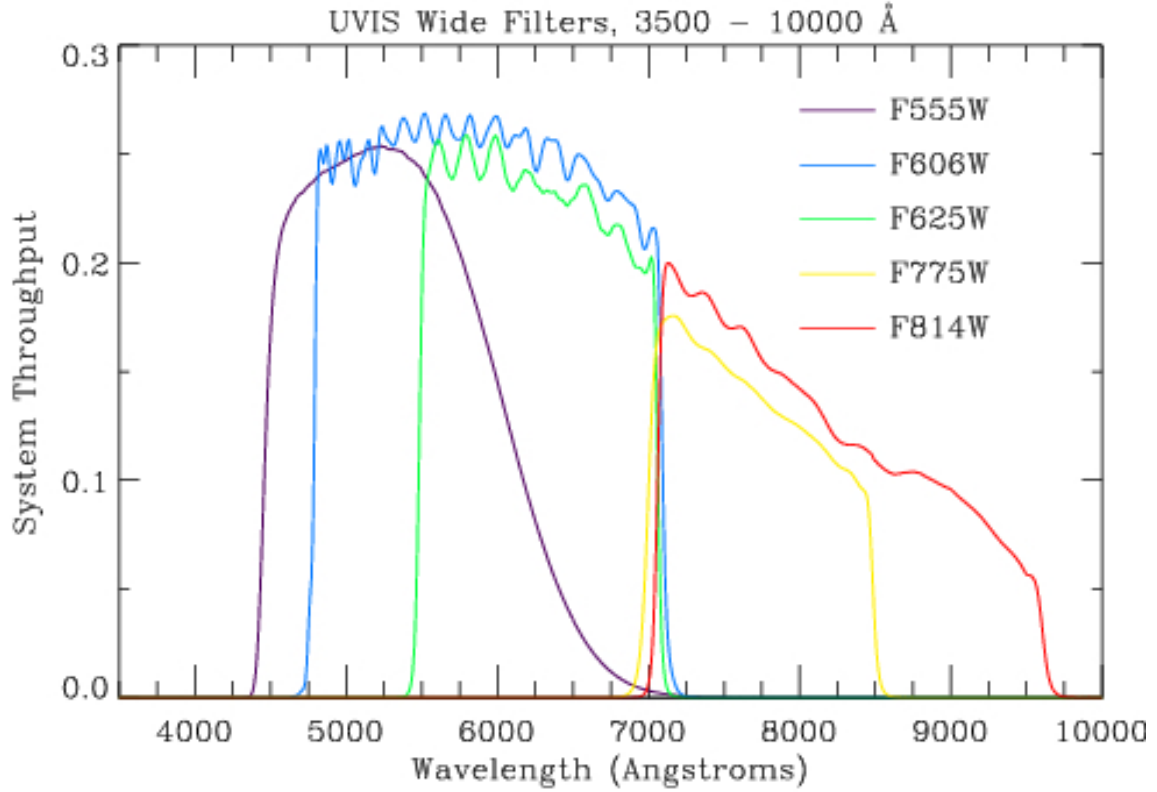


Figure 2.5: Filter response functions for wide-field WFC3 filters. Source: [http://www.stsci.edu/hst/wfc3/ins\\_performance/throughputs/UVIS\\_filterthru.html](http://www.stsci.edu/hst/wfc3/ins_performance/throughputs/UVIS_filterthru.html)

had parallax distances further from the cluster centre than would be expected for any star cluster. The size of the final dataset balanced the need for maintaining sufficient data points, to achieve a valid comparison to the previous studies of NGC 6793, particularly GC18, and eliminating the most anomalous data, such as stars with parallaxes calculated as being negative (and therefore not physically feasible).

The isochrone fitting to the NGC 6793 was done by eye using a plot of the cluster's observed Gaia CMD, the position of each star corrected for its parallax distance. Using the values of  $E(B-V)$  and age from GC18, a standard-case isochrone was derived, again assuming a diffuse ISM (i.e.,  $R_V = 3.1$ ). The standard treatment was employed twice, creating a different isochrone each time. A coefficient calculated from  $(A_X/A_V)_{MS}$  was applied in one case and one calculated using  $(A_X/A_V)_{plat}$  in the other. The fitting process was carried out in sequential stages:

1. First, the upper main sequence of the FBER isochrone was fitted to that of the standard-case isochrone by varying the value of  $A_V$  used to calculate the final FBER value for each stellar object.

2. Next, the age of the FBER isochrone was varied to match the observed turn-off location in the NGC 6793 data as far as possible.
3. Finally, the FBER isochrone metallicity was varied in an attempt match the observed lower main-sequence.

The isochrone with the resulting parameters were then plotted alongside two standard-case isochrones, The resulting curves were compared to each other for accuracy with respect to the observational data.